Desalination and Water Treatment
www.deswater.com
doi: 10.5004/dwt.2021.27490

231 (2021) 131–142
August

Adsorption of toluene from aqueous solutions onto polyethylene glycol modified bentonite: kinetic, isotherm studies and artificial neural network modeling

Nabil Bougdah[a,b,*], Nabil Messikh[a], Salim Bousba[c,d], Fayçal Djazi[a,b], Pierre Magri[e], Marek Rogalski[e]

[a]*Département de Pétrochimie et Génie des Procédés, Faculté de Technologie, Université 20 Août 1955-Skikda, Algérie, emails: n.bougdah@univ-skikda.dz (N. Bougdah), nabchem@yahoo.fr (N. Messikh), djazi_faycal@yahoo.fr (F. Djazi)*
[b]*LRPCSI, Université 20 Août 1955-Skikda, Algérie*
[c]*Département de Génie des Procédés, Faculté de Génie des Procédés, Université Salah Boubnider Constantine 3, Algérie, email: salim.bousba@univ-constantine3.dz*
[d]*Laboratoire Médicament et Développement Durable (REMEDD) Université Constantine 3, Constantine, Algérie*
[e]*LCP-A2MC, Université de Lorraine, 1, bd Arago-57078 METZ, Cedex 3, France, emails: pierre.magri@univ-lorraine.fr (P. Magri), rogalski@univ-metz.fr (M. Rogalski)*

Received 21 February 2021; Accepted 2 June 2021

ABSTRACT

In this work, Algerian natural bentonite was used in the preparation of a new adsorbent by impregnation with polyethylene glycol (PEG) for the removal of toluene from an aqueous solution. These interactions have been monitored by thermal method (thermogravimetric analysis) as well as by Fourier-transform infrared spectroscopy. The adsorption efficiency of natural and PEG-bentonite was examined for toluene removal by batch adsorption experiments under different operating conditions. Therefore, a multilayer perceptron (MLP) neural network was then used to predict the adsorption capacity of toluene. Different training algorithms were compared to determine the most suitable training algorithm. A single hidden with six neurons using a tangent sigmoid function transfer with the Levenberg–Marquardt backpropagation algorithm has been found the best predictive performance. The high value of coefficient determination (0.999) and low value of root mean square error (0.00074) proved that the MLP model can predict the adsorption capacity of toluene with reasonable accuracy. Furthermore, the sensitivity analysis based on the MLP model indicated that the contact time and the initial concentration of adsorbate with the same relative importance a round of 39% appeared to be the most influential parameter in the adsorption capacity of toluene, followed by adsorbent dose (20.99%).

Keywords: Adsorption; Bentonite; Polyethylene glycol; Toluene; Artificial neural network

1. Introduction

Hazardous aromatic hydrocarbons such as toluene are the major water-soluble constituents of gasoline that contaminate water and soil [1]. Toluene is a colorless, mobile liquid with an aromatic odor. It is practically insoluble in water (0.535 g L^{-1} at 25°C), miscible with many organic solvents (acetone, diethyl ether, chloroform, ethanol,...), soluble in glacial acetic acid. It is an excellent solvent for a large number of natural or synthetic substances (oil, greases and resins) [2–4].

The removal of the presence of toluene in drinking and other processed water is of significant importance and interest. Among processes employed in water treatment,

* Corresponding author.

adsorption is an important method with high removal efficiency and no harmful by-products. Numerous studies on toluene adsorption were published in the literature and various aspects of the adsorption mechanism were studied [5–7]. Recently, researchers have focused on using new efficient and recyclable adsorbents such as clays [8–11]. In recent years, organo-bentonite, an alternative adsorbent, has become the subject of study by many researchers [12–16].

Minerals can interact with substrates through a variety of mechanisms including intercalation. The guest molecule substrates enter between the mineral layers to expand the spacing between the mineral networks. Once these bonding networks have been expanded, the guest molecule is substituted further by polymeric materials.

Polyethylene glycol (PEG) is a widely available polymer with unique properties such as thermal stability, commercial availability, non-volatility, immiscibility with water and several organic solvents, and recyclability [17]. PEG is polar, miscible in water and compatible with aqueous clay mineral suspensions, and interacts at the molecular level. The intercalation of PEG in clay minerals involves an ion exchange reaction resulting in the occupation of an interlayer space of the clay structure [18].

The mechanism of the adsorption process is complex due to the interaction of many variables, and thus, the resulting relationships are highly nonlinear [19]. Therefore, conventional mathematical modeling cannot be used to fully model and simulate the adsorption data. To overcome this problem arising in the adsorption process, we explore the applicability of artificial neural networks (ANN), which are capable of approximating any continuous nonlinear functions to arbitrary accuracy, to predict the adsorption capacity of toluene from aqueous solution. One of the characteristics of modeling based on ANNs is that it does not require a mathematical description of the phenomena involved in the process [20]. Recently, ANNs have been widely applied in many engineering disciplines including the adsorption process [21–25].

The ANN is a computer-based technology that simulates a biological neuronal system with similar characteristics in terms of structural architecture and functional proprieties. The ANN model consists of many neurons that are interconnected and arranged in layers. The optimum ANNs structure is developed by training the model using experimental data from which it learns correlation patterns between the inputs and outputs data sets [26]. The performance of ANNs models is evaluated and compared in terms of nonlinear error functions which are statistically significant and measure the error distribution [27].

Given the above, this study aims to test the ability of modified and natural Algerian bentonite clays to adsorb toluene from water. The Algerian bentonite was modified with polyethylene glycol (PEG) for removing toluene as a toxic organic pollutant from aqueous solutions by the adsorption process. The effects of some parameters on the adsorption process, such as initial toluene concentration, adsorbent dose, and contact time, were examined. In addition, the capability of the ANN model was investigated to predict the adsorption capacity of toluene on modified bentonite. The artificial neural network model was also developed to study the adsorption process and the accuracy of the model was tested using correlation coefficient (R^2) and root mean squared error (RMSE).

2. Materials and methods

2.1. Preparation of adsorbate

Toluene, also known as methylbenzene or phenylmethane is an aromatic hydrocarbon having a molecular structure as C_7H_8 (with a molecular weight of 92.14 g mol^{-1}) was used in this work. The stock toluene solution was prepared by dissolving accurately weighed toluene of analytical grade in the deionized water to the concentration of 5 mmol L^{-1} and subsequently, the experimental solutions of various initial concentrations (C_0) were prepared by diluting the stock solution to the desired concentrations.

2.2. Preparation of PEG-bentonite

In this study, the used Algerian natural bentonite was from Hammam Boughrara (West of Algeria). The chemical properties of bentonite were well studied and published in the literature [1,28–30]. The chemical composition was as follows: SiO_2 – 69.4%, Al_2O_3 – 14.7%, Fe_2O_3 – 1.2%, MgO – 1.1%, CaO – 0.3%, Na_2O – 0.5%, K_2O – 0.8%, TiO_2 – 0.2%, As – 0.05%, and loss of ignition was 11% [31]. The polymer used is polyethylene glycol (PEG-3000). The bentonite was intercalated with PEG-3000 according to the same experimental procedure described for the intercalation of kaolinite with PEG [32]: 20 g of bentonite was stirred with 200 g of melted polyethylene glycol, a highly hydrophilic polymer. The temperature was held at 150°C for a total of 216 h (9 d).

2.3. Characterization of the adsorbent

The characteristics of the PEG-bentonite clay were analyzed using thermogravimetric analysis (TGA) and Fourier-transform infrared spectroscopy (FTIR). The thermal decomposition of PEG-bentonite was studied using thermal balance 2050 TGA V5.4 A from TA Instruments. The chemical modification of PEG-bentonite was confirmed by the FTIR spectra obtained by a spectrophotometer (Spectrum One FTIR spectrometer of PerkinElmer, USA) in the wavenumber range of 4,000–650 cm^{-1}.

2.4. Batch adsorption experiments

In the present study, the rates of adsorption of toluene were determined with bentonite and PEG-bentonite. 80 mg of the natural bentonite or PEG-bentonite at 25°C was added to 100 mL of the aqueous solution of toluene.

Solutions were stirred at 250 rpm during selected laps of time. Then, the solution was centrifuged to removing the clay dispersion and the residual toluene concentrations analyzed using the UV-Vis spectrometry at 206 nm wavelength. The solution concentration allowed to calculating the quantity q_t (mmol g^{-1}) of the toluene adsorbed by 1 g of bentonite or PEG-bentonite. All experiments were carried out in duplicate at neutral initial pH of solution (pH = 7) and the average value of the concentration was used for further calculation.

The solution concentration allowed us to calculate the quantities q_t (mmol g^{-1}), q_e (mmol g^{-1}) and, R (%) [33–35].

$$q_t = \left(C_0 - C_t\right) \times \frac{V}{m} \tag{1}$$

$$q_e = \left(C_0 - C_e\right) \times \frac{V}{m} \tag{2}$$

$$R(\%) = \frac{\left(C_0 - C_e\right)}{C_0} \times 100 \tag{3}$$

where q_t and q_e are the adsorption capacities of the toluene at the selected time t and at the equilibrium, respectively. R (%) is the percentage removal of toluene. C_0 and C_t (mmol L^{-1}) are the initial concentration and the concentration at the selected time t, respectively, of the toluene in the solution. V (L) is the volume of the toluene solution and m (g) is the mass of the used bentonite or PEG-bentonite.

2.5. Artificial neural network

ANN is a mathematical model similar to the structure of brain synaptic connections for information processing. It has become the focus of much attention, largely because of its wide applicability and ease with which can treat complicated problems [36]. In this research, an ANN model, feed-forward neural network namely multilayer perceptron (MLP) was used to predict the adsorption capacity of toluene on modified bentonite. Fig. 1 shows the arrangement of feed-forward multilayer perceptron network in the prediction of adsorption capacity of toluene on modified bentonite.

The simple architecture of MLP consists of an input layer, one or more hidden layer(s), and output layers. These hidden layers are composed of several neurons. The neurons of input and output layers are the same as the number of input and output parameters of the model. Universal approximation theory suggests that a network with one hidden layer with a sufficiently large number of neurons can be interpreted any input-output structure [15].

In this set of networks, information moves forward in merely one direction from the input layer toward the hidden layer and finally to the output. Running a neural network is normally carried out in two stages, namely learning or training and testing.

Among the various kinds of ANN approaches that exit, the backpropagation (BP) learning algorithm, which has become the most popular in engineering applications. This algorithm uses the supervised training technique where the network weights and biases are initialized randomly at the beginning of the training phase. The structure of the MLP model consists of three neurons in the input layer corresponding to the three operating variables (time, adsorbent dose, and the initial concentration of adsorbate), the output layer has one neuron corresponding to adsorption capacity (q_e). The number of hidden neurons is determined during the training process. Different training backpropagation algorithms were evaluated and trained, using the experimental data, to choose the best topology of the multilayer feedforward network and comment on their performance.

The dataset was classified into training and test sets which contained 80% and 20% of data experimental respectively. The complete data has been normalized in the range of (–1, 1) using Eq. (4):

$$x_{\text{norm}} = 2\frac{x_i - x_{\min}}{x_{\max} - x_{\min}} - 1 \tag{4}$$

where x_{norm} is the normalized value of x_i, with $x_{\min}$ and $x_{\min}$ being the minimum and maximum values of a certain variable, respectively.

The statistical indicators RMSE and R^2 are given by:

$$\text{RMSE} = \sqrt{\frac{1}{n}\sum_{i=1}^{n}\left(y_{i0} - y_i\right)^2} \tag{5}$$

$$R^2 = 1 - \frac{\sum_{i=1}^{n}\left(y_{i0} - y_i\right)^2}{\sum_{i=1}^{n}\left(y_{i0} - \bar{y}_i\right)^2} \tag{6}$$

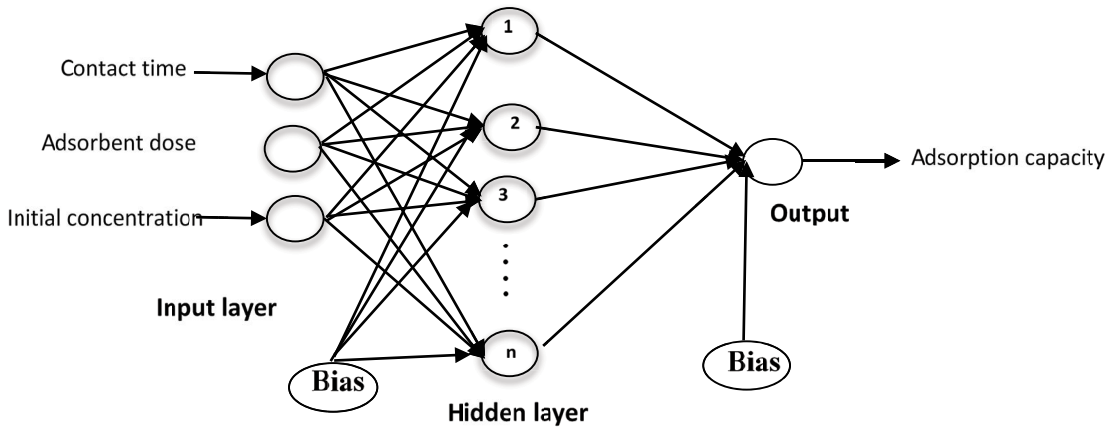

Fig. 1. Arrangement of the multilayer perceptron (MLP) artificial neural network.

where y_{i0} is the target output value, y_i is the neural network output and n is the total number of data patterns used.

3. Results and discussion

3.1. Characterization of the adsorbent

3.1.1. Thermogravimetric analyses

The results of the Thermal decomposition are illustrated in Fig. 2. The TGA records of the bentonite are shown in Fig. 2a, the mass loss of 8.689% corresponding to the dehydration of these clays was observed at 80.66°C. The TGA thermal curve that corresponds to PEG-bentonite (Fig. 2b), comprises two stages of the mass loss process. The first weight loss is about 0.708% caused by the release of the adsorbed water at 72.07°C. The second one corresponding to the PEG decomposition at 370.58°C with mass losses of 27.04%.

3.1.2. FTIR analysis

The FTIR spectra of natural bentonite and PEG-bentonite were taken in the range of 4,000–650 cm^{-1}. FTIR spectroscopy is very sensitive to modification of the clay structure upon PEG treatment as illustrated in Fig. 3.

Fig. 3a displays a typical spectrum of bentonite with the intense band at 982.79 cm^{-1} from stretching vibration of SiO, the other bands corresponding to the water sorbed by the bentonite: the υ2 H–O–H bending vibration spectral range at 1,630–1,740 cm^{-1}; υ1 H-bonding to Si–O–Al is located

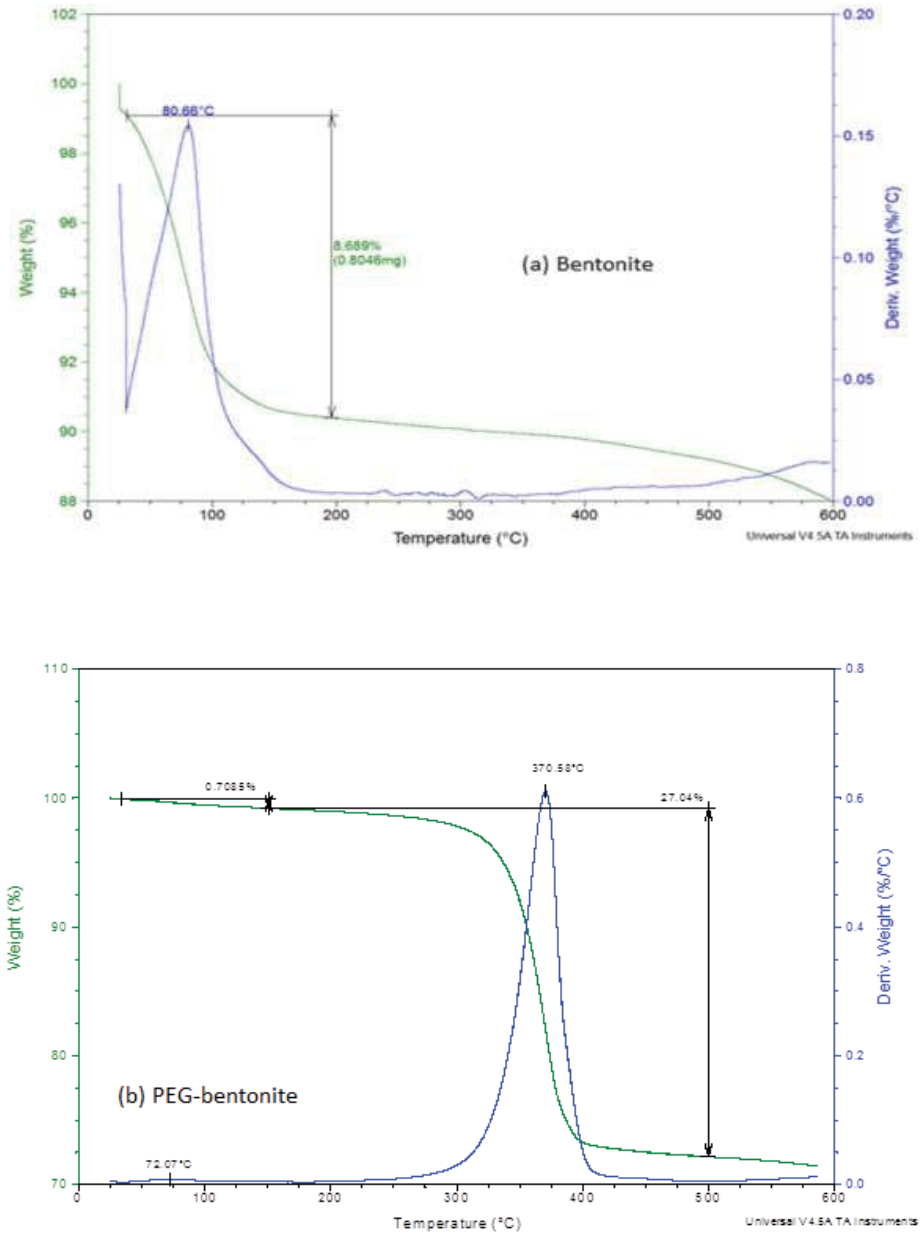

Fig. 2. TGA/DTG analysis of bentonite (a) and PEG-bentonite (b).

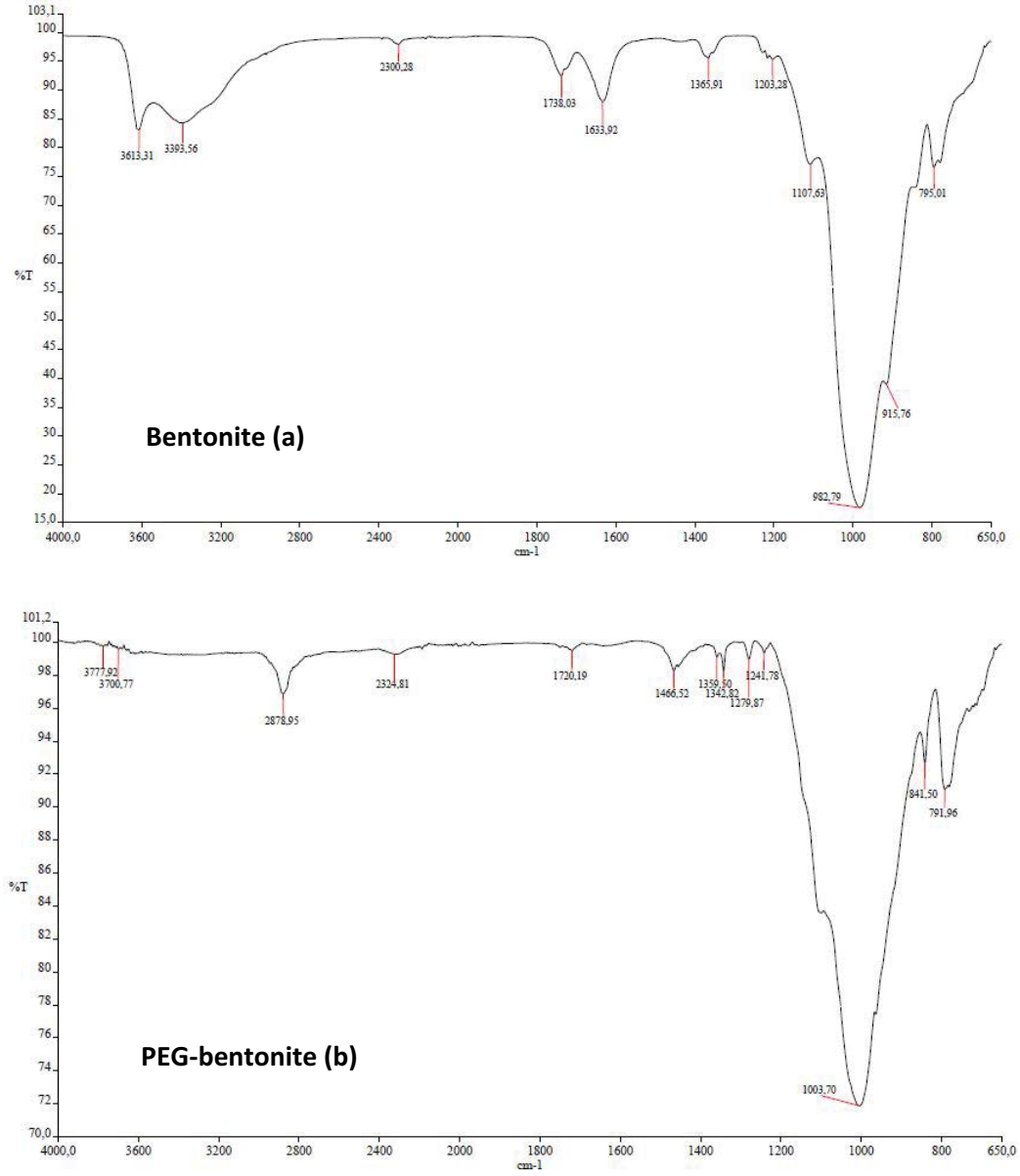

Fig. 3. Infrared spectra of bentonite (a) and PEG-bentonite (b).

at 3,390–3,620 cm^{-1} and the hydrogen bond to Si–O–Si linkage is located at 3,613 cm^{-1}.

The interaction between PEG polymeric chain and bentonite layer would cause changes in the corresponding region between 3,600 and 3,000 cm^{-1} (Fig. 3b). Additionally, the PEG add peak in the CH stretch region near 2,880 cm^{-1}, with the PEG peak being extremely broad. Other CH_2 wagging and C–C stretching bands are seen in the 1,240–1,360 cm^{-1} range for PEG-bentonite. This was possibly due to PEG-bentonite interaction [37].

3.2. Adsorption kinetics studies

Kinetic experiments were carried out in Erlenmeyer flasks including a 100 mL aqueous solution of toluene with a quantity of bentonite or PEG-bentonite at ambient temperature. Solutions were stirred at 250 rpm during selected laps time. After that, the solution was centrifuged to remove the clay dispersion and analyzed by UV spectrometry.

Fig. 4 presents the kinetics adsorption obtained at room temperature with a toluene initial concentration of 0.25 mmol L^{-1}. The mass of bentonite or PEG-bentonite was 80 mg within all experiments.

Fig. 4 shows the variation of the adsorbed toluene amount as a function of time on bentonite and PEG-bentonite. It can be seen from Fig. 4 that the adsorption capacity for both bentonite and PEG-bentonite gradually increases with time until equilibrium was reached. The results indicate that the contact time to reach the adsorption equilibrium is approximately 180 min for both adsorbents.

The experimental adsorption capacity at the equilibrium of toluene onto PEG-bentonite (0.2165 mmol g^{-1}) is almost higher than the adsorption of bentonite (0.1786 mmol g^{-1}).

Kinetic studies are important to estimate the adsorption efficiency of toluene and the mechanism of the sorption process onto PEG-bentonite and bentonite. Constants from kinetic models, pseudo-first-order (PFO), pseudo-second-order (PSO), and intraparticle diffusion model were fit for experimental data to examine the adsorption of toluene by bentonite and PEG-bentonite. The first one was the linear form of the pseudo-first-order model of Lagergren [38,39], generally expressed as follows:

$$\log\left(q_e - q_t\right) = \log\left(q_e\right) - \left(\frac{K_1}{2.303}\right)t \tag{7}$$

where q_e and q_t are the amounts of toluene adsorbed at equilibrium and after time t respectively. The rate constant of adsorption was noted as K_1 (min^{-1}). If the plot of $\log(q_e - q_t)$ vs. time is linear, then the value of K_1 may be directly obtained from the slope.

The PSO model [40,41] can be written as follows:

$$\frac{dq_t}{dt} = K_2\left(q_e - q_t\right)^2 \tag{8}$$

where K_2 is the equilibrium rate constant of the PSO model (g $mmol^{-1}$ min^{-1}). Separating the variables in Eq. (8) and integrating for the boundary conditions $q_t = 0$ to $q_t = q_t$ and $t = 0$ to $t = t$ yields an expression that may be rearranged into the following linear form:

$$\frac{t}{q_t} = \frac{1}{k_2 \times q_e^2} + \frac{t}{q_e} \tag{9}$$

The slope and the intercept allow establishing q_e and K_2 respectively.

The PFO and PSO models were used to fit, by linear regression, the experimental data of toluene adsorption onto bentonite and PEG-bentonite (figures not shown). The PFO and PSO rate constants K_1 and K_2 and the values of the predicted q_e ($q_{e,cal.}$) were calculated, and are given in Table 1.

The values of the coefficient of determination R^2 and the standard deviation (SD) Δq_e (%) for both models are also calculated and grouped in Table 1. The standard deviation (SD) Δq_e (%) is calculated between the experimental q_e ($q_{e,exp.}$) and the predicted q_e ($q_{e,cal.}$). The validity of PFO or PSO models can be determined by the calculation of the standard deviation (SD) Δq (%) and the coefficient of determination R^2 [42]. As can be seen from Table 1, in the case of bentonite the R^2 value for the PFO model was equal to the R^2 of the PSO model (0.99). On the contrary, in the case of PEG-bentonite, the R^2 of the PSO model was (0.98) higher than that for the PFO model (0.93). On the other hand, and for both bentonite and PEG-bentonite, the predicted q_e ($q_{e,cal.}$) obtained by the PFO model are closer to the experimental data than the predicted q_e values obtained by the PSO model. This observation is confirmed by the values of the standard deviation (SD) Δq_e (%) in Table 1. Based on the above noted, the PFO kinetic model is more accurate to describe the adsorption process of toluene onto both bentonite and PEG-bentonite.

To have a deeper insight into the mechanism of adsorption, the kinetic data was treated with an intraparticle diffusion model (IPD) proposed by Weber and Morris [43,44]. The IPD model is based on the expression obtained by solving second Fick's equation for an adsorbent particle suspended in solution:

$$q_t = K_{di} \times t^{1/2} + C_i \tag{10}$$

where K_{di} is the intraparticle diffusion rate constant (mmol g^{-1} $min^{-1/2}$) and C_i (mmol g^{-1}) is a constant that indicates the thickness of the boundary layer, that is, the higher the value of C_i, the greater the boundary layer effect.

If the plot of q_t vs. $t^{1/2}$ gives a straight line, this means that the adsorption of toluene is only controlled by the

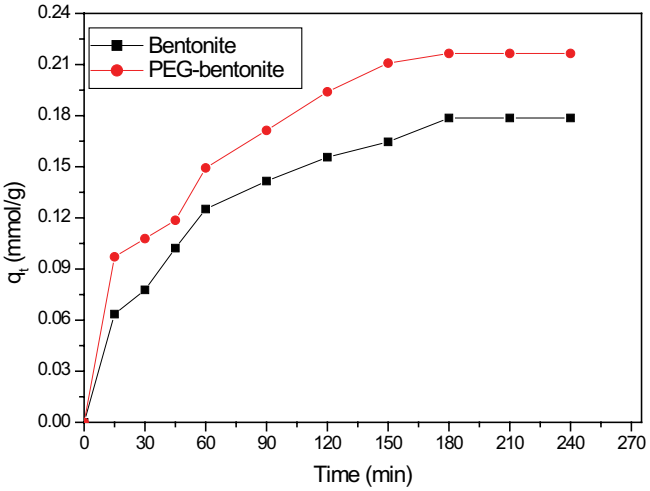

Fig. 4. Kinetics of adsorption the toluene on bentonite and PEG-bentonite.

Table 1
PFO and PSO kinetics models parameters for toluene adsorption

		PFO model				PSO model			
Adsorbent	$q_{e,exp.}$	K_1	$q_{e,cal.}$	Δq_e (%)	R^2	K_2	$q_{e,cal.}$	Δq_e (%)	R^2
Bentonite	0.179	0.016 ± 0.001	0.151 ± 0.003	15.64	0.99	0.094 ± 0.008	0.220 ± 0.009	22.90	0.99
PEG-bentonite	0.216	0.021 ± 0.002	0.224 ± 0.023	3.70	0.93	0.089 ± 0.013	0.264 ± 0.016	22.22	0.98

intraparticle diffusion mechanism. However, if the plot exhibit multi-lines, this means that two or more mechanism influence the toluene adsorption process [15–45].

Fig. 5 plots the number of moles of toluene adsorbed per unit mass of both bentonite (a) and PEG-bentonite (b) vs. $t^{0.5}$. Two straight lines were expected, which shows that intraparticle diffusion is not the only mechanism limiting the adsorption kinetics of toluene.

The intraparticle diffusion constants can be calculated using Eq. (10). Table 2 shows the intraparticle diffusion constants (K_{di} and C_i) for the two stages of the adsorption and the correlation coefficient (R^2). From Table 2, it can be seen that the order of the adsorption rate of toluene onto bentonite was higher in the first stage (K_{d1}) than in the second stage (K_{d2}). On the contrary, the order of the adsorption rate of toluene onto PEG-bentonite was higher in the second stage (K_{d2}) than in the first stage (K_{d1}) for which there was a significant change in the slope. Thus, the changes in K_{d1} and K_{d2} confirm that the adsorption mechanism of toluene on PEG-bentonite is different from that of the adsorption on natural bentonite.

3.3. Effect of adsorbent dose

The effect of adsorbent dose on the removal efficiency of toluene by bentonite or PEG-bentonite was investigated at toluene initial concentration of 0.25 mmol L^{-1}, and contact time of 180 min. The results are shown in Fig. 6.

According to the results in Fig. 6, by increasing adsorbent dose from 20 to 150 mg/100 mL, the toluene removal

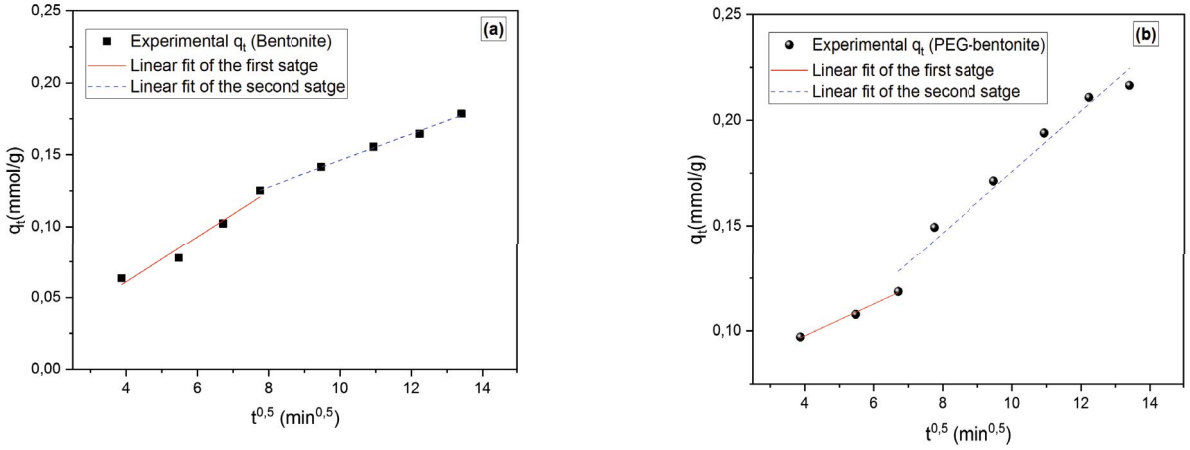

Fig. 5. Intraparticle diffusion model for toluene adsorption onto bentonite (a) and PEG-bentonite (b).

Table 2
Intraparticle diffusion model constants for toluene adsorption

Adsorbent	First stage			Second stage		
	K_{d1} (mmol g^{-1} min^{-1})	C_1	R_1^2	K_{d2} (mmol g^{-1} min^{-1})	C_2	R_2^2
Bentonite	0.016 ± 0.002	–0.003 ± 0.014	0.958	0.009 ± 3.27E-4	0.054 ± 0.003	0.996
PEG-bentonite	0.007 ± 5.9E-4	0.067 ± 0.003	0.994	0.014 ± 0.001	0.032 ± 0.013	0.966

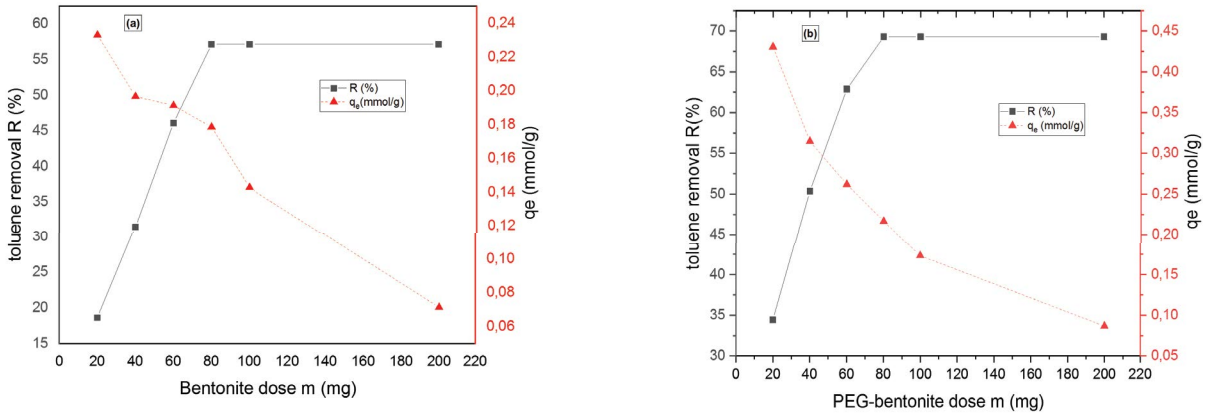

Fig. 6. Effect of the adsorbent dose of bentonite (a) and PEG-bentonite (b).

efficiency increased from 18.64% to 57.16% for bentonite and 34.44% to 69.28% for PEG-bentonite, whereas the adsorption capacity decreases from 0.233 to 0.071 mmol g^{-1} for bentonite and from 0.430 to 0.086 mmol g^{-1} for PEG-bentonite. Above 80 mg/100 mL of adsorbent dose, there was no significant increase in the removal rate of toluene R%, but the adsorption capacity q_e decreased rapidly. Considering q_e and R%, an adsorbent dose of 80 mg/100 mL was found to be the optimum bentonite and PEG-bentonite dose and was used for all other experiments. In fact, the percentage removal of toluene increases by increasing the adsorbent dosage, due to the increasing number of available surface-active sites of adsorbent. However, after a certain dosage, the percentage removal of toluene remains constant. This result is usually due to the presence of a large number of available surface-active sites compared to the constant adsorbate concentration [41].

3.4. Adsorption isotherms

An adsorption isotherm describes the mechanism of retention of the toluene to bentonite or PEG-bentonite at a constant temperature and pH. Adsorption equilibrium is established when the ratio between the adsorbed amount with the remaining in the solution becomes constant. The graphical representation of adsorption isotherms provides an insight into the adsorption mechanism, as well as the affinity of the adsorbate/adsorbent couple. Usually, the mathematical correlation of adsorption isotherm parameters yields an important tool for the analysis of the adsorption mechanism. Equilibrium isotherms for toluene adsorption onto bentonite or PEG-bentonite were obtained experimentally at neutral solution initial pH (pH = 7) for different initial concentrations of toluene ranging from 0.1 to 1 mmol L^{-1}.

3.4.1. Langmuir isotherm model

The Langmuir model was tested to describe the adsorption equilibrium of toluene onto bentonite or PEG-bentonite. The Langmuir equation can be written as follows [46]:

$$q_e = q_m \frac{K_L C_e}{1 + K_L C_e} \tag{11}$$

where q_m (mmol g^{-1}) is the theoretical maximum monolayer adsorption capacity and K_L (L $mmol^{-1}$) is the Langmuir constant.

The dimensionless separation factor R_L gives an idea of the favorability of the adsorption process. In fact, according to R_L value, the shape of Langmuir isotherm is evaluated to be favorable ($0 < R_L < 1$), unfavorable ($R_L > 1$), irreversible ($R_L = 0$) or linear adsorption ($R_L = 1$) [47,48]. The smaller R_L value indicates highly favorable adsorption. R_L values are calculated using the following equation [49]:

$$R_L = \frac{1}{1 + K_L C_0} \tag{12}$$

3.4.2. Freundlich isotherm model

The Freundlich model is expressed as follows [50]:

$$q_e = K_F \times C_e^{1/n} \tag{13}$$

where K_F and n are Freundlich constants, with K_F (L g^{-1}) indicating the adsorption capacity and n (dimensionless) indicating the favorable nature of the adsorption process. In reality, the Freundlich exponent ($1/n$) explains the type of isotherm, when ($1/n > 1$) the adsorption is unfavorable, ($1/n = 1$) the adsorption is homogeneous and ($0 < 1/n < 1$) the adsorption is favorable [51–53].

3.4.3. Henry's isotherm model

The Henry adsorption isotherm used to determine the equilibrium state of adsorption of secluded adsorbates at relatively low concentration with a linear expression [54,55]. Henry's adsorption isotherm model is represented as [56]:

$$q_e = K_H \times C_e \tag{14}$$

where K_H is Henry's adsorption binding constant of the adsorbate on the adsorbate surface;

The plots of q_e vs. C_e according to the non-linear form of Langmuir and Freundlich models and linear form of Henry's model were shown in Fig. 7a–c respectively.

The Langmuir and Freundlich parameters are calculated by non-linear regression analysis of the corresponding isotherms. Henry's parameter K_H is calculated by linear regression method.

The parameters of the Langmuir isotherm model are presented in Table 3. From Table 3, the obtained correlation coefficients (R^2) for the Langmuir model are low (0.97 for bentonite and 0.94 for PEG-bentonite) which indicates that the Langmuir model is not representative of the experimental adsorption data of toluene on both bentonite and PEG-bentonite. The parameters of Freundlich and Henry's isotherms are presented in Table 4. As shown in Table 4, R^2 values of Freundlich isotherm are very close to unity (0.999 for bentonite and 0.995 for PEG-bentonite) and are higher than that of Henry's isotherm (0.980 for bentonite and 0.991 for PEG-bentonite). This showed that the Freundlich model was more suitable for the adsorption process of bentonite and PEG-bentonite, indicating multilayer adsorption of toluene occurred on a heterogeneous bentonite surface with a non-uniform distribution of heat of adsorption [57]. In the Freundlich isotherm, the value of $1/n$ for the PEG-bentonite was less than 1 ($1/n = 0.909$), indicating that the adsorption is favorable, but for the bentonite, $1/n$ was equal to 1.242, indicating that the adsorption is unfavorable.

3.5. Artificial neural network modeling

An MLP model was developed in this present work. This model consists of an input layer with three neurons (parameters operatories), a hidden layer, and an output layer with one neuron (adsorption capacity). The number of neurons in the hidden layer was optimized by trial and error in

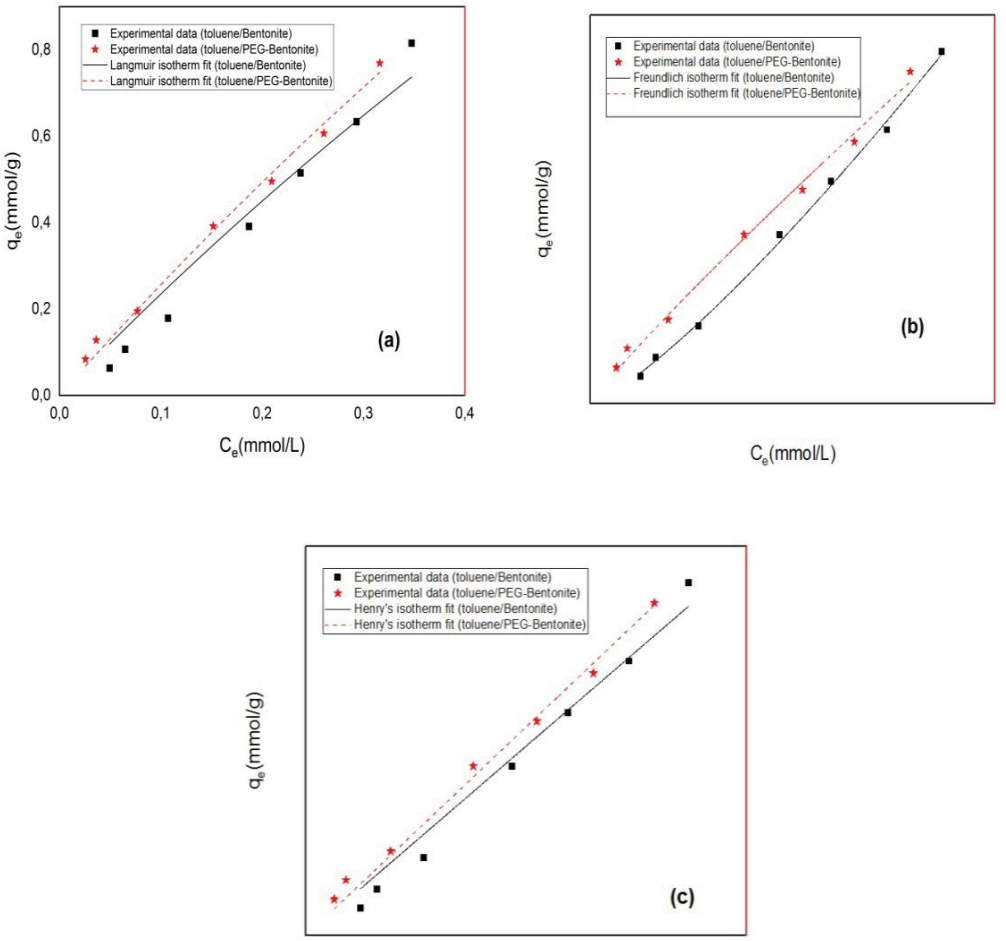

Fig. 7. Langmuir (a), Freundlich (b), and Henry's (c) isotherms representations of toluene adsorption onto bentonite or PEG-bentonite.

Table 3
Langmuir adsorption isotherms constants

Adsorbents	Langmuir isotherm			
	q_m	K_L	R_L	R^2
Bentonite	1.035 ± 0.253	1.335 ± 0.092	0.882 – 0.428	0.97
PEG-bentonite	2.641 ± 0.817	1.350 ± 0.105	0.881 – 0.425	0.94

Table 4
Freundlich and Henry's adsorption isotherms constants

Adsorbents	Freundlich isotherm			Henry isotherm	
	$1/n$	K_F	R^2	K_H	R^2
Bentonite	1.242 ± 0.024	3.013 ± 0.155	0.999	2.193 ± 0.072	0.980
PEG-bentonite	0.909 ± 0.054	2.363 ± 0.156	0.995	2.685 ± 0.054	0.991

order that the error between experimental values and predicted values is minimized. Selecting the proper algorithm and the transfer function is a very important step for designing an ANN model. Therefore, six backpropagation (BP) algorithms were applied to training an MLP network with a tangent sigmoid (tansig) transfer function at the hidden layer and a linear transfer function (purelin) at the output layer. The MLP model selected 16 (80%) of input data as training

and the remaining 4 (20%) as testing data sets. The structure of MLP was optimized based on RMSE and R^2 values.

Table 5 shows that the Levenberg–Marquardt backpropagation algorithm gives the most satisfactory results. As shown in Table 5, the smallest RMSE was obtained about 0.00075 for trainlm function. However, the other backpropagation algorithms also give satisfactory results but with greater RMSE than Levenberg–Marquardt algorithm. In addition, the RMSE remains constant even if the number of neurons in the hidden layer increases as shows in Fig. 8. The loss of the optimality of the estimates/results produced by some BP training algorithms can be attributed to the combinatorial nature and nonlinear structure of experimental data [58].

To have a more precise investigation into the model, regression analysis between outputs and the desired target was performed as shown in Fig. 9. There is a high correlation between the predicted value by the MLP model and the experimental data. The correlation coefficient was 0.999, in the analysis of the whole network, which implies that the model satisfactory in the adsorption capacity of toluene on modified bentonite.

In order to evaluate the relative importance of different input variables, on the adsorption capacity of toluene, the sensitivity analysis was conducted based on the neural net weight matrix and Garson equation [59]. The relative importance is calculated as follows:

$$I_j = \frac{\sum_{m=1}^{m=N_h}\left[\left(\frac{\left|W_{jm}^{ih}\right|}{\sum_{k=1}^{N_i}\left|W_{km}^{ih}\right|}\right)\left|W_{mn}^{ho}\right|\right]}{\sum_{k=1}^{k=N_i}\left\{\sum_{m=1}^{m=N_h}\left[\left(\frac{\left|W_{km}^{ih}\right|}{\sum_{k=1}^{N_i}\left|W_{km}^{ih}\right|}\right)\left|W_{mn}^{ho}\right|\right]\right\}} \quad (15)$$

where I_j is the relative importance of the jth input variable on the output variable, N_i and N_h are the numbers of input and hidden neurons, respectively. W is connection weights, the superscripts 'i', 'h' and 'o' refer to input, hidden and output layers, respectively, and subscripts 'k', 'm' and 'n' refer to input, hidden and output neurons, respectively.

Based on the results, the contact time and the initial concentration of adsorbate with the same relative importance a round of 39% appeared to be the most influential parameters in the adsorption process modified bentonite for toluene removal (Fig. 10), followed by adsorbent dose (21%).

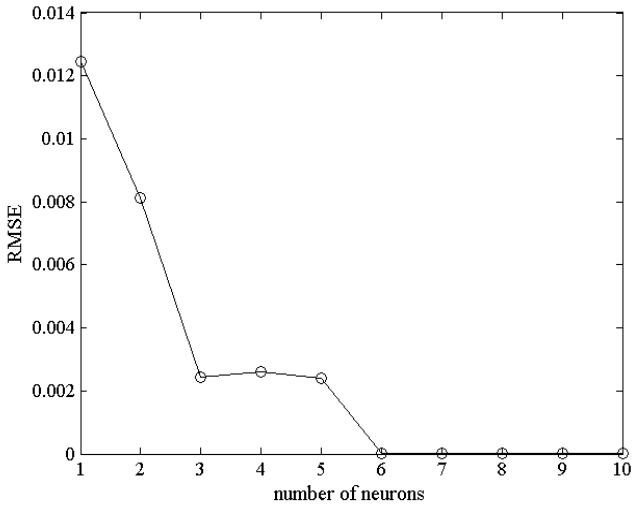

Fig. 8. Relation between RMSE and number neurons in hidden layer for trainlm algorithm.

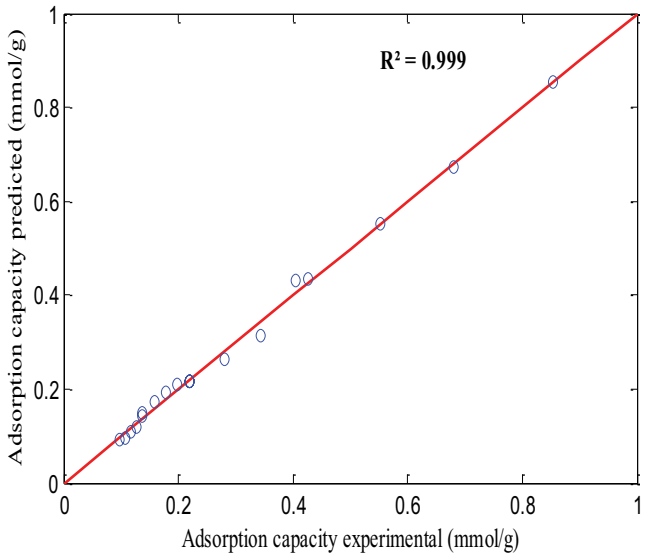

Fig. 9. Comparison between experimental and predicted adsorption capacity of adsorbent.

Table 5
Summary of trial and error method used for adsorption capacity MLP model development

Backpropagation (BP) algorithms	Function	Number of neurons optimal in hidden layer	RMSE	R^2
Bayesian regularization	trainbr	2	0.00409	0.9998
Levenberg–Marquardt backpropagation	trainlm	6	0.00075	0.9999
Fletcher–Reeves conjugate gradient backpropagation	trainf	8	0.00939	0.9990
Polak–Ribière conjugate gradient backpropagation	traincgp	7	0.01183	0.9983
Powell–Beale conjugate gradient backpropagation	traingb	2	0.009698	0.9889
Batch gradient descent	traingd	8	0.02608	0.9919

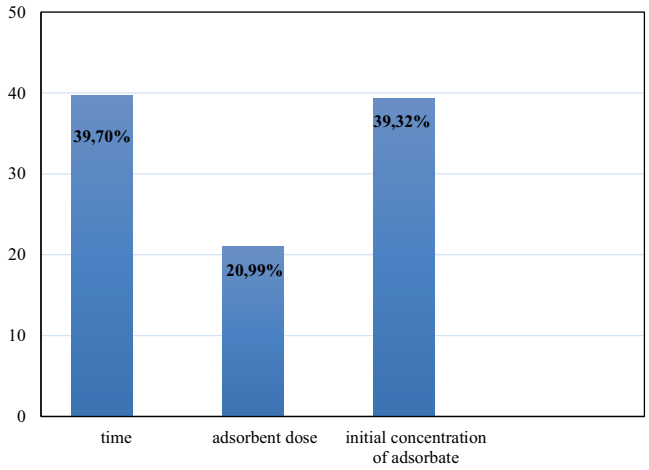

Fig. 10. Relative importance of the input variables on the adsorption capacity of toluene.

However, many researchers proved that the influential variable and effect of each variable depended upon the experimental ranges adopted in the fitting model [20].

4. Conclusion

The bentonite and modified PEG-bentonite were found to be efficient as a low-cost adsorbent for the removal of organic compounds such as toluene from aqueous solutions. This experiment shows that PEG can be intercalated into minerals such as bentonite. These new materials were characterized using FTIR and TGA techniques. Modified clays as a PEG-bentonite were developed to improve their adsorption properties. According to the results, bentonite and PEG-bentonite are effective clay-sorbents for removal of toluene from aqueous solutions. Higher of toluene removal efficiency values were obtained with modified PEG-bentonite. The experimental quantity of adsorbed toluene ranged from 0.1786 mmol g^{-1} for bentonite to 0.2165 mmol g^{-1} for PEG-bentonite, which means that the adsorption capacity of PEG-bentonite is greater than that of natural bentonite.

The adsorption data of toluene onto bentonite or PEG-bentonite at equilibrium are fitted well with the Freundlich model. The kinetic study reveals that the mechanism of adsorption of toluene on PEG-bentonite is different from that of natural bentonite.

Moreover, the performance of the MLP model in the prediction of adsorption capacity was investigated using six learning backpropagation algorithms. By means of trial and error, the best topology of the MLP model was chosen as six neurons in the hidden layer with tangent sigmoid function transfer and Levenberg–Marquardt learning algorithm. The proposed MLP model showed a precise and effective prediction of experimental data with a high value of the coefficient of determination (0.999) and a low value of root mean square error (0.00075), which can be applied successfully applied to modeling the adsorption of toluene on the modified bentonite. In addition, sensitivity analysis demonstrated that, the contact time and the initial concentration of adsorbate with the same relative importance a round of 39%.

References

[1] F. Sekrane, Z. Bouberka, A.K. Benabbou, M. Rabiller-Baudry, Z. Derriche, Adsorption of toluene on bentonites modified by dodecyltrimethylammonium bromide, Chem. Eng. Commun., 198 (2011) 1093–1110.
[2] Toluene – European Union Risk Assessment Report, Vol. 30, European Chemicals Bureau, Publications Office of the EU, 2003. Available at: echa.europa.eu
[3] K. Othmer, Encyclopedia of Chemical Technology, 5th ed., Vol. 25, John Wiley and Sons, New York, 2007, pp. 350–389.
[4] NIOSH Criteria Documents, Criteria for a Recommended Standard: Occupational Exposure to Toluene, The National Institute for Occupational Safety and Health (NIOSH), DHHS (NIOSH) Publication Number 73-11023, U.S. Department of Health & Human Services, USA, 1973.
[5] A. Erto, S. Chianese, A. Lancia, D. Musmarra, On the mechanism of benzene and toluene adsorption in single-compound and binary systems: energetic interactions and competitive effects, Desal. Water Treat., 86 (2017) 259–265.
[6] G. Chen, K. Song, X. Huang, W.B. Wang, Removal of toluene and Pb(II) using a novel adsorbent modified by titanium dioxide and chitosan, J. Mol. Liq., 295 (2019) 111683, doi: 10.1016/j.molliq.2019.111683.
[7] T. Chenet, E. Sarti, V. Costa, A. Cavazzini, E. Rodeghero, G. Beltrami, S. Felletti, L. Pasti, A. Martucci, Influence of caffeic acid on the adsorption of toluene onto an organophilic zeolite, J. Environ. Chem. Eng., 8 (2020) 104229, doi: 10.1016/j.jece.2020.104229.
[8] J.V. Fernandes, A.M. Rodrigues, R.R. Menezes, G. de Araújo Neves, Adsorption of anionic dye on the acid-functionalized bentonite, Materials (Basel), 13 (2020) 3600, doi: 10.3390/ma13163600.
[9] T. Bakalár, M. Kaňuchová, A. Girová, H. Pavolová, R. Hromada, Z. Hajduová, Characterization of Fe(III) adsorption onto zeolite and bentonite, Int. J. Environ. Res. Public Health, 17 (2020) 5718, doi: 10.3390/ijerph17165718.
[10] I. Robles, Y. Bandala, J. Manríquez, E. Bustos, Modeling of Hg(II) adsorption onto Ca-bentonite, J. Mex. Chem. Soc., 62 (2018) 305–313.
[11] P. Liu, L.X. Zhang, Adsorption of dyes from aqueous solutions or suspensions with clay nano-adsorbents, Sep. Purif. Technol., 58 (2007) 32–39.
[12] I. Fatimah, T. Huda, Preparation of cetyltrimethylammonium intercalated Indonesian montmorillonite for adsorption of toluene, Appl. Clay Sci., 74 (2013) 115–120.
[13] C. Obi, U.N. Okike, P.I. Okoye, The use of organophilic bentonite in the removal phenol from aqueous solution: effect of preparation techniques, Mod. Chem. Appl., 6 (2018) 258, doi: 10.4172/2329-6798.1000258.
[14] Q. Kang, W.Z. Zhou, Q. Li, B.Y. Gao, J.X. Fan, D.Z. Shen, Adsorption of anionic dyes on poly(epicholorohydrin dimethylamine) modified bentonite in single and mixed dye solutions, Appl. Clay Sci., 45 (2009) 280–287.
[15] Y.H. Shu, L.S. Li, Q.Y. Zhang, H.H. Wu, Equilibrium, kinetics and thermodynamic studies for sorption of chlorobenzenes on CTMAB modified bentonite and kaolinite, J. Hazard. Mater., 173 (2010) 47–53.
[16] R. Ocampo-Perez, R. Leyva-Ramos, J. Mendoza-Barron, R.M. Guerrero-Coronado, Adsorption rate of phenol from aqueous solution onto organobentonite: surface diffusion and kinetic models, J. Colloid Interface Sci., 364 (2011) 195–204.
[17] E. Rajanarendar, K.G. Reddy, M.N. Reddy, S. Raju, K.R. Murthy, Polyethylene glycol (PEG) mediated synthesis of pyrrolo-[2,3-*d*]isoxazoles by using NaOCl reagent – a green chemistry approach, Green Chem. Lett. Rev., 4 (2011) 257–260.
[18] G.A. Seilkhanova, A.N. Imangaliyeva, Y. Mastai, A.B. Rakhym, Bentonite polymer composite for water purification, Bull. Mater. Sci., 42 (2019) 1–8.
[19] N. Prakash, S.A. Manikandan, L. Govindarajan, V. Vijayagopal, Prediction of biosorption efficiency for the removal of copper(II) using artificial neural networks, J. Hazard. Mater., 152 (2008) 1268–1275.
[20] A.R. Khataee, M.B. Kasiri, Artificial neural networks modeling of contaminated water treatment processes by homogeneous

and heterogeneous nanocatalysis, J. Mol. Catal. A: Chem., 331 (2010) 86–100.
[21] S. Chowdhury, P.D. Saha, Artificial neural network (ANN) modeling of adsorption of methylene blue by NaOH-modified rice husk in a fixed-bed column system, Environ. Sci. Pollut. Res., 20 (2013) 1050–1058.
[22] A.M. Ghaedi, V. Vafaei, Applications of artificial neural networks for adsorption removal of dyes from aqueous solution: a review, Adv. Colloid Interface Sci., 75 (2017) 20–39.
[23] Y. Yang, X. Lin, B. Wei, Y. Zhao, J. Wang, Evaluation of adsorption potential of bamboo biochar for metal-complex dye: equilibrium, kinetics and artificial neural network modelling, Int. J. Environ. Sci. Technol., 11 (2014) 1093–1100.
[24] B.R. Broujeni, A. Nilchi, F. Azadi, Adsorption modeling and optimization of thorium (IV) ion from aqueous solution using chitosan/TiO_2 nanocomposite: application of artificial neural network and genetic algorithm, Environ. Nanotechnol. Monit. Manage., 15 (2021) 100400, doi: 10.1016/j.enmm.2020.100400.
[25] M. Maghsoudi, M. Ghaedi, A. Zinali, A.M. Ghaedi, M.H. Habibi, Artificial neural network (ANN) method for modeling of sunset yellow dye adsorption using zinc oxide nanorods loaded on activated carbon: kinetic and isotherm study, Spectrochim. Acta, Part A, 134 (2015) 1–9.
[26] L. Das, U. Maity, J.K. Basu, The photocatalytic degradation of carbamazepine and prediction by artificial neural networks, Process Saf. Environ. Prot., 92 (2014) 888–895.
[27] R.R. Karri, J.N. Sahu, activated carbon: error analysis of linear and non-linear methods, J. Taiwan Inst. Chem. Eng., 80 (2017) 472–487.
[28] S. Guergazi, D. Amimeur, S. Achour, Elimination des substances humiques de deux eaux de surface algériennes par adsorption sur charbon actif et sur bentonite, Larhyss J., 13 (2013) 125–137.
[29] N. Bougdah, P. Magri, A. Modaressi, F. Djazi, R. Zaghdoudi, M. Rogalski, Suitable organoclays for removing slightly soluble organics from aqueous solutions, J. Chem. Pharm. Res., 7 (2015) 295–306.
[30] R. Sennour, G. Mimane, A. Benghalem, S. Taleb, Removal of the persistent pollutant chlorobenzene by adsorption onto activated montmorillonite, Appl. Clay Sci., 43 (2009) 503–506.
[31] H. Khalaf, O. Bouras, V. Perrichon, Synthesis and characterization of Al-pillared and cationic surfactant modified Al-pillared Algerian bentonite, Microporous Mater., 8 (1997) 141–150.
[32] J.J. Tunney, C. Detellier, Aluminosilicate nanocomposite materials. Poly(ethylene glycol) − kaolinite intercalates, Chem. Mater., 8 (1996) 927–935.
[33] N. Bougdah, N. Messikh, S. Bousba, F. Djazi, P. Magri, M. Rogalski, Removal of chlorobenzene by adsorption from aqueous solutions on the HDTMA-bentonites as a function of HDTMA/CEC ratio, Curr. Res. Green Sustainable Chem., 3 (2020) 100038, doi: 10.1016/j.crgsc.2020.100038.
[34] R. Tayebee, V. Mazruy, Acid-thermal activated nanobentonite as an economic industrial adsorbent for malachite green from aqueous solutions. Optimization, isotherm, and thermodynamic studies, J. Water Environ. Nanotechnol., 3 (2018) 40–45.
[35] M.F. Mota, M.G.F. Rodrigues, F. Machado, Oil–water separation process with organoclays: a comparative analysis, Appl. Clay Sci., 99 (2014) 237–245.
[36] N.G. Turan, B. Mesci, O. Ozgonenel, The use of artificial neural networks (ANN) for modeling of adsorption of Cu(II) from industrial leachate by pumice, Chem. Eng. J., 171 (2011) 1091–1097.
[37] J.J. Perez, M.E. Villanueva, L. Sánchez, R. Ollier, V. Alvarez, G.J. Copello, Low cost and regenerable composites based on chitin/bentonite for the adsorption potential emerging pollutants, Appl. Clay Sci., 194 (2020) 105703, doi: 10.1016/j.clay.2020.105703.
[38] I. Kahoul, N. Bougdah, F. Djazi, C. Djilani, P. Magri, M.S. Medjram, Removal of methylene blue by adsorption onto activated carbons produced from agricultural wastes by microwave induced KOH activation, Chem. Chem. Technol., 13 (2019) 365–371.
[39] F. Rahmawati, V. Natalia, A.T. Wijayanta, K. Nakabayashi, J. Miyawaki, S. Rondiyah, Carbon waste powder prepared from carbon rod waste of zinc-carbon batteries for methyl orange adsorption, Bull. Chem. React. Eng. Catal., 15 (2020) 66–73.
[40] S.M. Mousavi, A. Babapoor, S.A. Hashemi, B. Medi, Adsorption and removal characterization of nitrobenzene by graphene oxide coated by polythiophene nanoparticles, Phys. Chem. Res., 8 (2020) 225–240.
[41] S. Bousba, N. Bougdah, N. Messikh, P. Magri, Adsorption removal of humic acid from water using a modified Algerian bentonite, Phys. Chem. Res., 6 (2018) 613–625.
[42] H. Moussout, H. Ahlafi, M. Aazza, H. Maghat, Critical of linear and nonlinear equations of pseudo-first-order and pseudo-second-order kinetic models, Karbala Int. J. Mod. Sci., 4 (2018) 244–254.
[43] S. Chatterjee, M.W. Lee, S.H. Woo, Adsorption of congo red by chitosan hydrogel beads impregnated with carbon nanotubes, Bioresour. Technol., 101 (2010) 1800–1806.
[44] S. Ahmadi, C.A. Igwegbe, Adsorptive removal of phenol and aniline by modified bentonite: adsorption isotherm and kinetics study, Appl. Water Sci., 8 (2018) 170, doi: 10.1007/s13201-018-0826-3.
[45] H.Z. Boudiaf, M. Boutahala, S. Sahnoun, C. Tiar, F. Gomri, Adsorption characteristics, isotherm, kinetics, and diffusion of modified natural bentonite for removing the 2,4,5-trichlorophenol, Appl. Clay Sci., 90 (2014) 81–87.
[46] K. Mohanty, D. Das, M.N. Biswas, Adsorption of phenol from aqueous solutions using activated carbons prepared from *Tectona grandis* sawdust by $ZnCl_2$ activation, Chem. Eng. J., 115 (2005) 121–131.
[47] A. Günay, E. Arslankaya, I. Tosun, Lead removal from aqueous solution by natural and pretreated clinoptilolite: adsorption equilibrium and kinetics, J. Hazard. Mater., 146 (2007) 362–371.
[48] C.A. Igwegbe, O.D. Onukwuli, J.T. Nwabanne, Adsorptive removal of vat yellow 4 on activated *Mucuna pruriens* (velvet bean) seed shells carbon, Asian J. Chem. Sci., 1 (2016) 1–16.
[49] F. Arias, T.K. Sen, Removal of zinc metal ion (Zn^{2+}) from its aqueous solution by kaolin clay mineral: a kinetic and equilibrium study, Colloids Surf., A, 348 (2009) 100–108.
[50] H. Koyuncu, N. Yıldız, U. Salgın, F. Köroğlu, A. Çalımlı, Adsorption of *o*-, *m*- and *p*-nitrophenols onto organically modified bentonites, J. Hazard. Mater., 185 (2011) 1332–1339.
[51] D. Kim, K.S. Ryoo, A study on adsorption of Li from aqueous solution using various adsorbents, Bull. Korean Chem. Soc., 36 (2015) 1089–1095.
[52] K.G. Bhattacharyya, S.S. Gupta, G.K. Sarma, Interactions of the dye, Rhodamine B with kaolinite and montmorillonite in water, Appl. Clay Sci., 99 (2014) 7–17.
[53] A.K. Meher, S. Das, S. Rayalu, A. Bansiwal, Enhanced arsenic removal from drinking water by iron-enriched aluminosilicate adsorbent prepared from fly ash, Desal. Water Treat., 57 (2015) 20944–20956.
[54] Z.H. Wang, Y. Li, P. Guo, W.J. Meng, Analyzing the adaption of different adsorption models for describing the shale gas adsorption law, Chem. Eng. Technol., 39 (2016) 1921–1932.
[55] F.S. Nworie, F.I. Nwabue, W. Oti, E. Mbam, B.U. Nwali, Removal of methylene blue from aqueous solution using activated rice husk biochar: adsorption isotherms, kinetics and error analysis, J. Chilean Chem. Soc., 64 (2019) 4365–4376.
[56] J.J. Martínez-Vertel, A.P. Villaquirán-Vargas, Á. Villar-García, D.F. Moreno-Díaz, A.X. Rodríguez-Castelblanco, Polymer adsorption isotherms with NaCl and $CaCl_2$ on kaolinite substrates, Revista DYNA, 86 (2019) 66–73.
[57] K.E. Onwuka, J.C. Igwe, C.U. Aghalibe, A.I. Obike, Hexadecyltrimethyl ammonium (HDTMA) and trimethylphenyl ammonium (TMPA) cations intercalation of Nigerian bentonite clay for multi-component adsorption of benzene, toluene, ethylbenzene and xylene (BTEX) from aqueous solution: equilibrium and kinetic studies, J. Anal. Tech. Res., 2 (2020) 70–95.
[58] K. Yetilmezsoy, S. Demirel, Artificial neural network (ANN) approach for modeling of Pb(II) adsorption from aqueous solution by *Antep pistachio* (*Pistacia Vera* L.) shells, J. Hazard. Mater., 153 (2008) 1288–1300.
[59] G.D. Garson, Interpreting neural-network connection weights, AI Expert, 6 (1991) 47–51.